Neuron
NeuroResource

Generation of Human Striatal Neurons by MicroRNA-Dependent Direct Conversion of Fibroblasts

Matheus B. Victor,[1,2,6] Michelle Richner,[1,6] Tracey O. Hermanstyne,[1,3] Joseph L. Ransdell,[1,3] Courtney Sobieski,[2,4] Pan-Yue Deng,[5] Vitaly A. Klyachko,[5] Jeanne M. Nerbonne,[1,3] and Andrew S. Yoo[1,*]
[1]Department of Developmental Biology
[2]Program in Neuroscience
[3]Center for Cardiovascular Research
[4]Department of Psychiatry
Washington University School of Medicine, Saint Louis, MO 63110, USA
[5]Departments of Biomedical Engineering and Cell Biology and Physiology, CIMED, Washington University, Saint Louis, MO 63110, USA
[6]Co-first Authors
*Correspondence: yooa@wustl.edu
http://dx.doi.org/10.1016/j.neuron.2014.10.016

SUMMARY

The promise of using reprogrammed human neurons for disease modeling and regenerative medicine relies on the ability to induce patient-derived neurons with high efficiency and subtype specificity. We have previously shown that ectopic expression of brain-enriched microRNAs (miRNAs), miR-9/9* and miR-124 (miR-9/9*-124), promoted direct conversion of human fibroblasts into neurons. Here we show that coexpression of miR-9/9*-124 with transcription factors enriched in the developing striatum, BCL11B (also known as CTIP2), DLX1, DLX2, and MYT1L, can guide the conversion of human postnatal and adult fibroblasts into an enriched population of neurons analogous to striatal medium spiny neurons (MSNs). When transplanted in the mouse brain, the reprogrammed human cells persisted in situ for over 6 months, exhibited membrane properties equivalent to native MSNs, and extended projections to the anatomical targets of MSNs. These findings highlight the potential of exploiting the synergism between miR-9/9*-124 and transcription factors to generate specific neuronal subtypes.

INTRODUCTION

The generation of induced pluripotent stem cells (iPSCs) holds great promise for regenerative medicine and the study of human diseases (Takahashi and Yamanaka, 2006; Yu et al., 2007). Nevertheless, creating a reliable in vitro disease model based on deriving iPSCs from multiple human samples followed by differentiation into a specific cell subtype is a lengthy process, which can be further complicated by the variable and unpredictable nature across different iPSC lines (Hu et al., 2010). Moreover, reprogramming somatic cells to iPSCs has been shown to reintroduce the embryonic state and therefore hinders the prospect of modeling late-onset disorders, although new methods are being developed that may overcome this barrier (Lapasset et al., 2011; Miller et al., 2013). Most importantly, current differentiation protocols often produce a population of cells with variable heterogeneity (Soldner and Jaenisch, 2012). Bypassing pluripotency and directly reprogramming readily accessible human tissues, such as skin, into neural cells may offer a fast and efficient approach to study neurological disorders (Caiazzo et al., 2011; Pang et al., 2011; Yoo et al., 2011). Although direct neuronal conversion may offer unique benefits, this approach is currently limited to a small number of protocols to specify neuronal subtypes using postnatal or adult human samples (Caiazzo et al., 2011; Liu et al., 2013; Ring et al., 2012; Son et al., 2011; Yoo et al., 2011).

MiR-9/9* and miR-124 are critical components of a genetic pathway that controls the assembly of neuron-specific, ATP-dependent chromatin remodeling complexes during neural development (Staahl et al., 2013; Yoo et al., 2009). In addition, these miRNAs have been shown to play key roles in the differentiation of neural progenitors to mature neurons by regulating the expression of antineural genes (Makeyev et al., 2007; Packer et al., 2008; Visvanathan et al., 2007; Xue et al., 2013). Ectopic expression of miR-9/9*-124 promotes the direct conversion of human adult fibroblasts toward neurons, a process greatly enhanced by coexpressing transcription factors, NeuroD2, ASCL1, and MYT1L, yielding a mixed population of excitatory and inhibitory neurons (Yoo et al., 2011). It remained unknown, nonetheless, whether the miR-9/9*-124-mediated neuronal conversion could yield a homogeneous population of a discrete neuronal subtype. Since the terminally differentiated state of neuronal subtypes can be instructed by transcription factors (Hobert, 2011), we hypothesized that transcription factors enriched in distinct brain regions could guide the miRNA-mediated neuronal reprogramming into a specific neuronal subtype.

In this study, we describe the identification of four transcription factors, CTIP2, DLX1, DLX2, and MYT1L (CDM), that synergize with miR-9/9*-124 to generate an enriched population of cells characteristic of striatal medium spiny neurons (MSNs), the

primary cell type affected in Huntington's disease (Albin et al., 1989). Importantly, this reprogramming relies on the activities of miR-9/9*-124, since CDM factors alone are ineffective for neuronal conversion. This combinatorial approach generates a large number of neurons with a gene expression profile analogous to primary human striatal cells microdissected from postmortem brain sections. Furthermore, when transplanted into the mouse striatum, the reprogrammed neurons display functional properties similar to native MSNs. The high efficiency and specificity of our approach to directly derive human striatal MSNs will likely be advantageous in modeling disorders affecting MSNs such as Huntington's disease.

RESULTS

Enhancement of miR-9/9*-124-Mediated Reprogramming

We previously noticed that a large fraction of cells underwent cell death when transduced to express miR-9/9*-124 (Yoo et al., 2011). In an effort to optimize the miR-9/9*-124-mediated neuronal reprogramming, we tested if coexpression of an antiapoptotic gene would reduce the number of cells deaths during neuronal reprogramming. Previous studies have shown that abrogation of apoptosis could enhance neurogenesis (Sahay et al., 2011; Zhang et al., 2006) and that overexpression of an antiapoptotic gene *BCL2L1* (also known as *Bcl-xL*) suppressed programmed cell death (Alavian et al., 2011; Blömer et al., 1998). When we incorporated Bcl-xL into our lentiviral vector to be expressed with miR-9/9*-124 (Supplemental Experimental Procedures available online), we detected an increased number of surviving cells by over 40% and significantly improved the reprogramming efficiency (Figure S1). We utilized a doxycycline (Dox)-inducible promoter to temporarily regulate the expression of miR-9/9*-124 and Bcl-xL. Our characterization of the Dox-inducible promoter indicated that the transgene readily became inactive upon the removal of Dox within 3 days (Figure S2). We found that the continuous expression of miR-9/9*-124 for approximately 30 days was necessary for stable neuronal conversion as interrupting the transgene expression at day 15 resulted in a significant reduction in the neuronal conversion (Figure S2). Accordingly, in tissue culture as well as in experiments in vivo, we routinely withdrew Dox treatment after 30 days into reprogramming. Interestingly, we found that endogenous miR-9/9* and miR-124 were expressed after Dox removal by day 30 as the cells adopted a neuronal fate (Figure S2).

Identification of Transcription Factors to Specify Striatal Neurons

We focused on transcription factors expressed in the GABAergic MSNs of the striatum, a clinically relevant neuronal subtype affected in Huntington's disease (Albin et al., 1989). Striatum-enriched transcription factors were selected based on translational ribosome affinity purification data for DRD1- or DRD2-positive MSNs from the mouse striatum (Dougherty et al., 2010) and gene expression databases from Brainspan (http://brainspan.org) and Allen Brain Atlas (http://human.brain-map.org/). In order to identify transcription factors that would favor the MSN fate, we transduced human postnatal fibroblasts with lentivirus to express miR-9/9*-124 and sixteen selected transcription factors individually and examined by immunostaining the number of MAP2-positive cells that were also positive for the neurotransmitter GABA and the dopamine- and cAMP-regulated neuronal phosphoprotein (DARPP-32), a well-documented marker of MSNs (Arlotta et al., 2008; Lobo et al., 2006; Ouimet and Greengard, 1990) (Figures 1A and S3). BCL11B (also known as CTIP2), a transcription factor critical for the differentiation of MSNs in vivo (Arlotta et al., 2008), was the only factor tested with miR-9/9*-124 to yield DARPP-32-positive neurons (Figure 1A). Furthermore, when miR-9/9*-124 were combined with DLX1 and DLX2, previously shown to be important for terminal differentiation of MSNs (Anderson et al., 1997), we detected a large percentage of GABAergic neurons (72.3% of MAP2-positive cells) (Figure 1A). It is interesting to note that MYT1L, which has previously been used by our group and others to enhance direct neuronal reprogramming with other factors (Pang et al., 2011; Yoo et al., 2011), significantly increased the number of MAP2-positive cells when tested alone with miR-9/9*-124 (Figures 1A and S3). Importantly, single transcription factors tested without miR-9/9*-124 did not induce MAP2-positive cells (data not shown).

Immunostaining Analysis of Neuronal Markers

Based on our initial screening of individual transcription factors, we asked if the combination of CTIP2, DLX1, DLX2 (DLX1/2), and MYT1L (collectively termed CDM) would synergize with miR-9/9*-124 to generate MSN-like cells (Figure 1A). We first determined if miR-9/9*-124 with CDM (miR-9/9*-124-CDM) would robustly generate neurons by examining the expression of general neuronal markers, MAP2, TUBB3 (also known as β-III tubulin), and NeuN (Figure 1B). Counting random fields of view revealed that approximately 90% of DAPI-positive cells were MAP2-positive (n = 207), 87% TUBB3-positive (n = 328), and 84% NeuN-positive (n = 328) at 5 weeks posttransduction (Figure 1C). The converted cells also expressed proteins important for neuronal function, including voltage-gated sodium channels (Figure 1D, left) and Synapsin 1 (Figure 1D, right). The neuronal conversion was dependent on miR-9/9*-124 as transducing human fibroblasts with CDM factors alone was ineffective in generating neurons (0.3% MAP2-positive, n = 343) (Figure 1E). Moreover, expression of CDM in human fibroblasts did not induce the expression of endogenous neural microRNAs such as miR-9/9*, miR-124, or miR-132 (Figure S4).

Detection of Markers of Medium Spiny Neurons

We found that the majority of the converted cells were GABAergic neurons (90% of MAP2-positive, n = 474) assayed by immunostaining for GABA (Figure 1F, top left, and S5, top, for larger overview) and GAD67 (Figures 1F, top right, and S5), without VGLUT1-positive (a marker for glutamatergic neurons) cells within the population of reprogrammed neurons (0.75% of MAP2-positive cells, n = 400; Figure S6). Furthermore, we found that a large fraction of converted neurons (70% of MAP2-positive, n = 474) expressed DARPP-32 (Figures 1G and S7 for view of GABAergic DARPP-32-positive cells) and expressed FOXP1 and DLX5 (Figure 1F, bottom left and right, respectively; 1G for quantification; and S7 for larger fields of view), which are

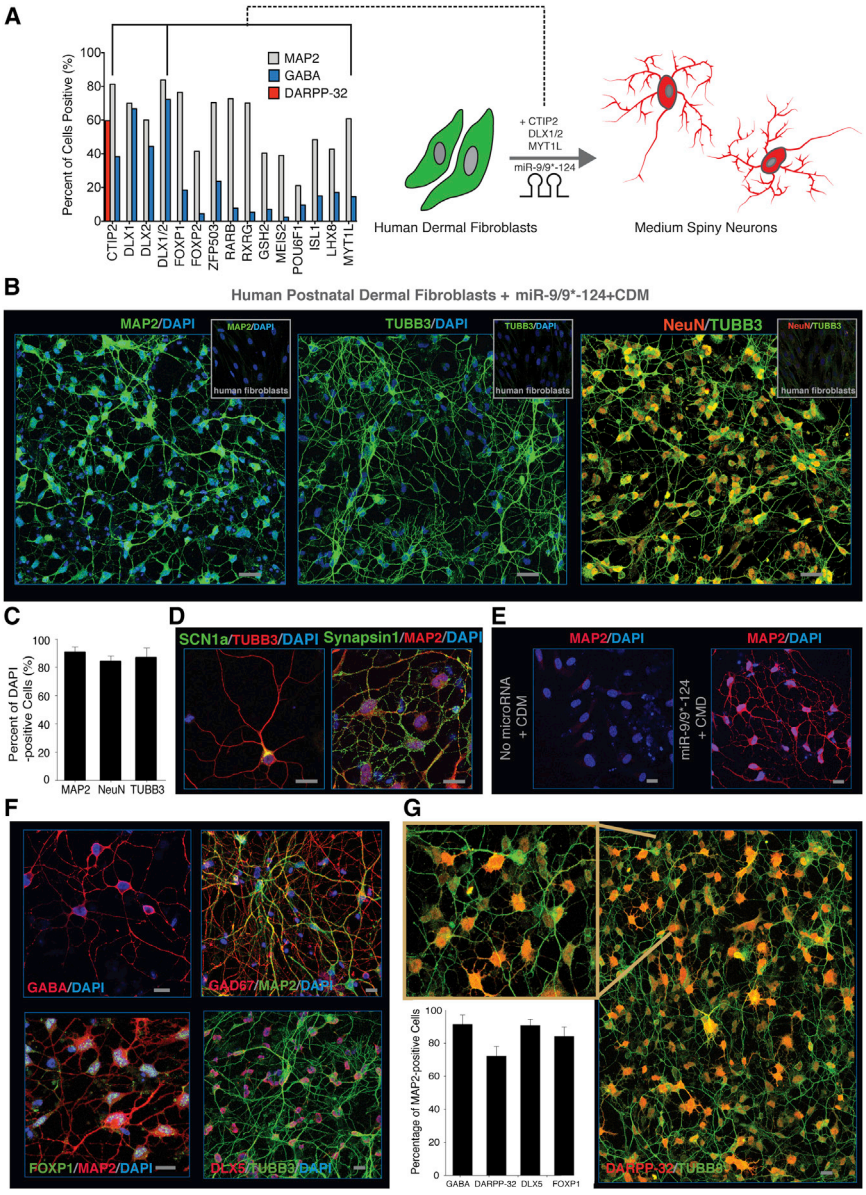

Figure 1. Neuronal Conversion of Human Fibroblasts by MicroRNAs and Striatal Factors

(A) Quantification by immunostaining of the synergistic effect of miRNAs and striatum-enriched factors represented by the percentage of human postnatal fibroblasts positive for MAP2, GABA, and DARPP-32 after 35 days of being transduced with miR-9/9*-124 in conjunction with striatum-enriched factors. On the right, diagram representing the ability of miR-9/9*-124 to generate striatal MSNs when combined with CTIP2, DLX1, DLX2, and MYT1L (CDM). (See Figure S3 for images of reprogrammed cells and other combinations attempted.)

(B) Expression of pan-neuronal markers, MAP2 (left), TUBB3 (middle), and NeuN (right) after neuronal conversion of human postnatal dermal fibroblasts with miR-9/9*-124 combined with transcription factors CDM. Larger scale views. Scale bar, 20 μm.

(C) Quantification of MAP2-, NeuN-, and TUBB3-positive cells for DAPI signals from randomly picked fields of view. For MAP2 and TUBB3 quantification, only the cells with processes at least three times the length of the cell body were counted positive. MAP2: n = 207 cells; TUBB3: n = 328 cells; NeuN: n = 328 cells. The error bars are in SD.

(D) Expression of SCN1a and Synapsin 1 in miR-9/9*-124-CDM-converted cells. Scale bar, 20 μm.

(E) Human postnatal fibroblasts transduced with CDM factors in the absence of miR-9/9*-124 did not generate neurons after 35 days, demonstrating the requirement of miR-9/9*-124 for neuronal conversion of human fibroblasts. Scale bar, 20 μm.

(F and G) Expression of markers of GABAergic MSNs. GABA ([E], top left) and GAD67 ([E], top right). FOXP1 ([E], bottom left), DLX5 ([E], bottom right), and DARPP-32 (G) are proteins enriched in MSNs. The inset represents a magnified view of (G). The graph (in [G], bottom left) represents quantification of GABA, FOXP1, DLX5, and DARPP-32 expression in MAP2-positive cells. GABA: n = 474 cells; FOXP1: n = 232 cells; DLX5: n = 207 cells; DARPP-32: n = 260 cells. The error bars are in SD. Figures S5 and S7 provide larger overviews of these markers as well as GABAergic DARPP-32-positive cells and controls.

also highly expressed in MSNs (Desplats et al., 2006; Ferland et al., 2003; Stenman et al., 2003; Tamura et al., 2004). In addition, we found that the endogenous *DLX1* was also expressed in cells converted by miR-9/9*-124-CDM (Figure S8). Reprogramming human fibroblasts using miR-9/9*-124 with DLX1/2 and MYT1L but without CTIP2 yielded highly GABAergic neurons that were completely devoid of DARPP-32 expression (Figure S9).

Interestingly, overexpression of CTIP2 (BCL11B) has been shown to protect hematopoietic progenitor cells from apoptosis, partially through the activity of members of the BCL2 family, including Bcl-xL (Albu et al., 2007). We therefore tested if ectopically expressing CTIP2 would induce the expression of *Bcl-xL* but found no significant changes (Figure S4).

Single-Cell Gene Expression Profiling

To further characterize the converted cells, we performed multiplex gene expression analyses in single cells to determine the enrichment of neuronal subtypes. Single cells induced from postnatal human fibroblasts were collected at 5 weeks posttransduction and identified based on the expression of housekeeping genes, *GAPDH*, *RSP18*, and *HPRT1* (Figure 2A, left marked by green dendrogram; n = 76 cells). Consistent with our immunostaining data, we found that the majority of the induced cells were positive for gene products expressed in neurons including *MAP2*, *TUBB3*, and *MAPT*, as well as components of voltage-gated sodium channels (*SCN2A* and *SCN3A*), neural cell adhesion molecule (*NCAM1*), neuronal ankyrin (*ANK2*), brain-derived neurotrophic factor (*BDNF*), and the synapse-associated protein

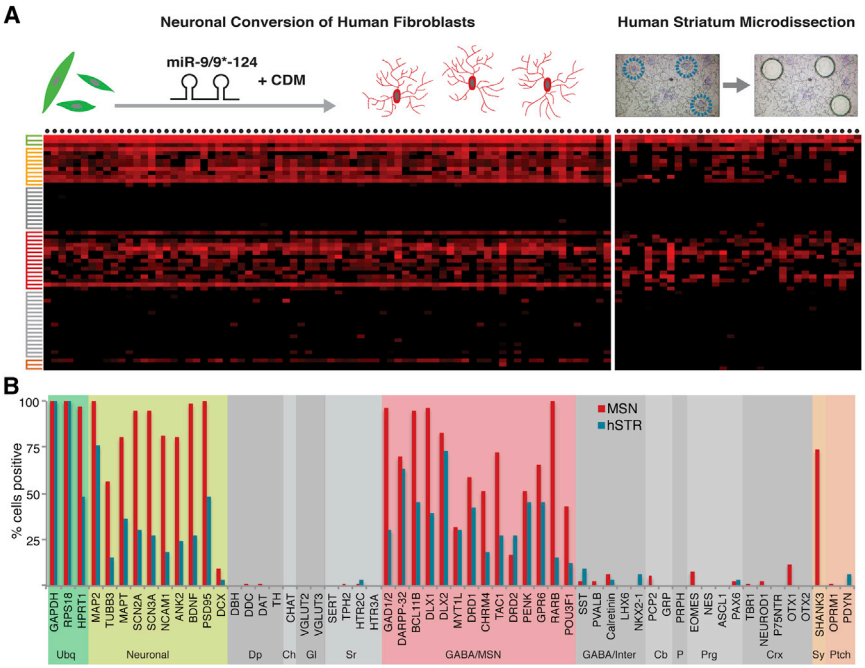

Figure 2. Single-Cell Gene Expression Analysis of Converted Cells and of Medium Spiny Neurons Microdissected from Human Adult Striatum

(A) Heatmap representation of multiplex qPCR of 76 converted cells (left) and 33 cells microdissected from postmortem human putamen sections (right). Each dot on top represents an individual cell and color-coded dendrograms denote genes of specific brain regions and cell types described in (B). Top illustrations represent the miR-9/9*-124-CDM-mediated neuronal conversion (left) and single-cell laser-microdissection of cresyl violet-stained human striatum sections (right).

(B) Quantification of percentages of converted cells and hMSNs for gene expression of specific neuronal types. Ubq: ubiquitous; Neuronal: genes generally expressed in neurons; Dp: dopaminergic; Ch: cholinergic; Gl: glutamatergic; Sr: serotonergic; GABA/MSN: GABAergic MSNs; GABA/Inter: GABAergic interneurons; Cb: cerebellum; P: peripheral nervous system; Prog: neural progenitors; Crx: cortical; Sy: presynaptic; Ptch: striatal patch. Figure S10 uses a pairwise comparison of these two sample groups to quantify the degree of similarity of gene expression profile.

PSD95 (also known as *DLG4*) (Figures 2A, left panel yellow dendrogram, and 2B, red bars). Interestingly, we did not detect the expression of doublecortin (*DCX*), a marker of immature, migratory neurons (Karl et al., 2005), suggestive of the maturity of the induced neurons. Importantly, miR-9/9*-124-CDM-induced cells were devoid of markers of dopaminergic neurons (*DBH*, *DDC*, *DAT*, and *TH*), cholinergic neurons (*CHAT*), glutamatergic neurons (*VGLUT2* and *VGLUT3*), and serotonergic neurons (*SERT*, *TPH2*, *HTR2C*, and *HTR3A*) (Figures 2A, left, gray dendrogram, and 2B). Instead, the majority of converted cells were positive for GABAergic markers (*GAD1*/*GAD2*) and *DARPP-32* (also known as *PPP1R1B*) in agreement with our immunostaining data. We also detected expression of genes associated with striatonigral (*DRD1*, *CHRM4*, and *TAC1*) and striatopallidal (*DRD2*, *PENK*, and *GPR6*) MSNs (Lobo et al., 2006) as well as transcription factors *RARB* and *POU3F1* (Figures 2A, left, red dendrogram, and 2B). *SHANK3*, which has been shown to be important for the synaptic function of MSNs (Peça et al., 2011), was also expressed in a high fraction of the converted cells. Interestingly, we did not detect expression of genes enriched in striatal patch neurons (*OPRM1* and *PDYN*) (Gong et al., 2003; Pert et al., 1976) in the converted cells. This suggests that the converted MSNs are likely to be of the striatal matrix (Figure 2B), which constitutes about 85% of the volume of the striatum (Johnston et al., 1990), consistent with the role of DLX1/2 in specifying matrix neurons (Anderson et al., 1997).

Human Striatum Laser Microdissection

To compare the gene expression profile of the converted cells to primary striatal neurons in the human brain, we analyzed human striatal cells collected by laser capture microdissection (LCM) from human postmortem adult striatal sections using the same set of assay primers. Consistent with the notion that the striatum is highly populated with MSNs (Gerfen, 1992), we detected that a large percentage of microdissected cells expressed *DARPP-32*. In addition, LCM samples expressed *CTIP2*, *DLX1*, *DLX2*, and *MYT1L*, and the overall gene expression profile was analogous to miR-9/9*-124-CDM-induced neurons (Figures 2A, right panel, and 2B, blue bars) (Figure S10 for pairwise comparison of LCM and reprogrammed MSNs). Importantly, miR-9/9*-124-CDM generated a homogenous population of MSNs, as we did not detect the expression of genes exclusive to striatal or cortical GABAergic interneurons (*SST*, *PVALB*, *Calretinin*, *LHX6*, and *NKX2-1)* (Marin et al., 2000; Tepper et al., 2010) (Figure 2). In both sets of data, genes enriched in the cerebellum (*PCP2* and *GRP*), peripheral nervous system (*PRPH*), neural progenitors (*EOMES*, *NES*, *ASCL1*, and *PAX6*), and in cortical neurons (*TBR1*, *NEUROD1*, *P75NTR*, *OTX1*, and *OTX2*) were also largely undetectable (Figure 2). Finally, a pairwise comparison of the expression of genes tested between the reprogrammed cells and microdissected human MSN (hMSN) indicated a strong correlation with a coefficient of determination (R squared) value of 0.77 (Figure S10). We also found miR-9/9* and miR-124 to be highly expressed in the human striatum (Figure S11), consistent with the expression of endogenous miR-9/9*-124 in converted MSNs (Figure S2).

Functional Properties of Reprogrammed hMSNs in Tissue Culture

The striatal circuitry is exceptionally intricate as it converges inputs from several brain regions with distinctive neurotransmitters, such as glutamatergic input from cortex and thalamus, dense dopaminergic innervation from substantia nigra, and local cholinergic and GABAergic inhibition (Graybiel et al., 1994). Many of these inputs have been shown to contribute to shaping the membrane properties and functional maturation of MSNs.

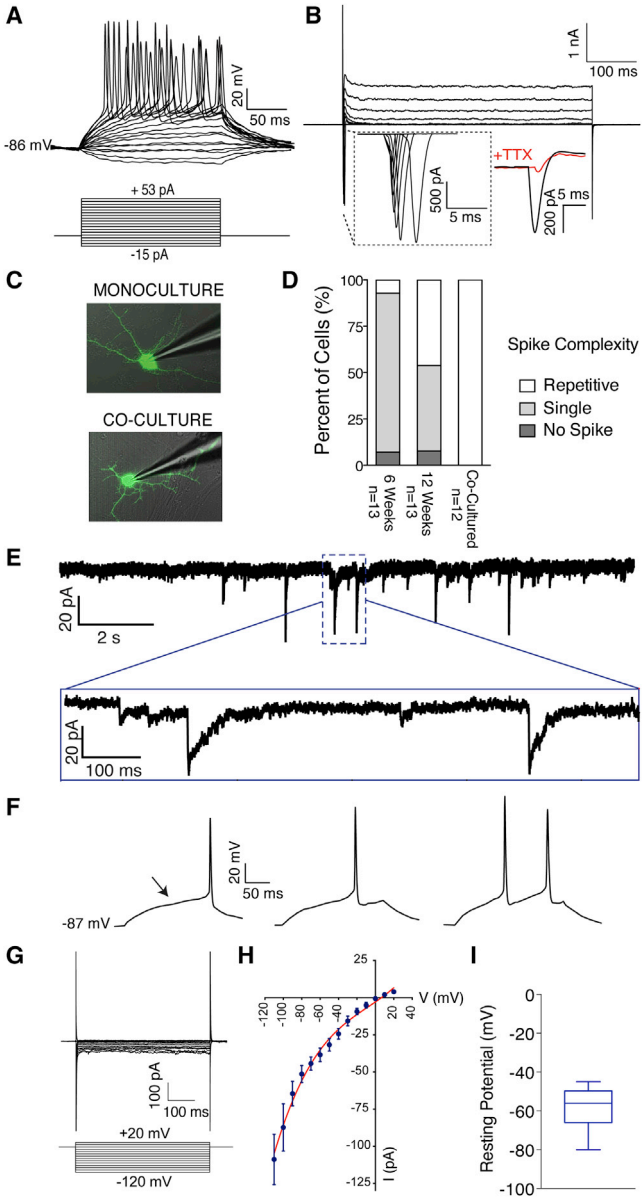

Figure 3. Electrophysiological Characteristics of Converted Medium Spiny Neurons in Tissue Culture

(A) Whole-cell current-clamp recording of MSNs converted from postnatal human fibroblasts. Converted human cells were cocultured with neonatal rat glia and displayed multiple APs in response to step current injections at 6 weeks posttransduction. All cells recorded (n = 12) fired APs in response to current injections.

(B) Representative traces of fast-inactivating inward currents recorded in voltage-clamp mode and blocked by 300 nM TTX. Voltage steps ranged from +10 to +70 mV.

(C and D) Increased complexity of AP spikes of converted cells when cocultured with glia. EGFP-tagged cells converted from postnatal fibroblasts were recorded at 6 or 12 weeks posttransduction. At 6 weeks, cells were recorded in the absence (monoculture) or presence of rat primary glia (coculture) (C). In monoculture, the majority of cells showed single spikes at 6 weeks posttransduction, whereas a larger percentage of cells recorded at 12 weeks generated repetitive APs. When cocultured with primary glia, all cells fired repetitively at 6 weeks (D). Intrinsic membrane properties are provided in Table S1.

For example, parvalbumin-expressing fast-spiking interneurons (PV-FSI) and neuropeptide-Y positive low-threshold spiking interneurons (NPY-LTS) have been shown to form synaptic connections with MSNs and regulate their firing activity (Do et al., 2012; Koós and Tepper, 1999). Therefore, MSNs can be distinguished in vivo not only due to their biochemical and anatomical differences but also by their intrinsic physiological properties. MSNs have been shown to rest at a hyperpolarized membrane potential (−80 mV to −90 mV), significant inwardly rectifying K^+ currents at or below resting membrane potentials, and a firing pattern with long delays to the initial action potential (AP) with little or no spike frequency accommodation (SFA) (Gertler et al., 2008; Venance and Glowinski, 2003). To examine the generic neuronal electrophysiological properties as well as MSN-specific properties in cells converted by miR-9/9*-124-CDM in tissue culture, we performed whole-cell patch-clamp recordings at 6 weeks posttransduction in converted cells cultured with rat primary glia. We found that all converted cells elicited multiple APs upon the injection of depolarizing currents (Figure 3A) and large fast-inactivating inward currents followed by outward potassium currents when evoked by a series of voltage steps (Figure 3B) (see Table S1 for intrinsic membrane properties) (n = 12). Inward currents were ablated upon local perfusion of tetrodotoxin (TTX) (300 nM), indicating that they were mediated via TTX-sensitive voltage-gated sodium channels (Figure 3B). To test the ability of converted cells to become electrically active in the absence of primary glia, we decided to investigate the membrane properties of our cells cultured in isolation (monoculture). Surprisingly, converted neurons were also capable of firing APs and displayed functional maturation over time in culture. Whereas the converted cells initially displayed modest APs at 6 weeks, a much more complex firing pattern with nearly 50% of the recorded cells firing repetitively was evident at 12 weeks posttransduction (shown in Figure 3D). In addition, converted cells displayed significantly larger peak amplitudes of inward currents at 12 weeks, correlated with increased excitability (see Figure S12 and Table S1 for additional traces and membrane properties). Since one of the major inputs impinging upon MSNs in vivo are excitatory glutamatergic afferents from the cerebral cortex (Kreitzer, 2009), we investigated if coculturing the converted cells with rat cortical neurons would lead to the formation of functional synapses. As seen by the synaptic currents (Figure 3E) (8 out of 13 total cells recorded), reprogrammed MSNs successfully mature into synaptically active neurons. In addition to determining that the reprogrammed cells are

(E) Representative trace of spontaneous postsynaptic currents from cocultured cells recorded at 12 weeks.

(F) Deconstructed traces from current-clamp recording shown in (A). The first spike event, followed by sequential steps is shown from left to right. Arrow denotes a latency to the initial spike characteristic of MSNs.

(G) Representative traces of inward rectifying currents generated from whole-cell voltage-clamp recording. Cells were stimulated with voltage steps ranging from −120 mV to +20 mV in 10 mV increments.

(H) Current levels at steady state were measured and plotted against holding voltages to generate an I-V curve fitted with a cubic spline curve (displayed in red) (n = 7).

(I) Resting membrane potentials of recorded cells (n = 12). Box and whisker plot is shown to represent the median as well as the greatest and lowest value.

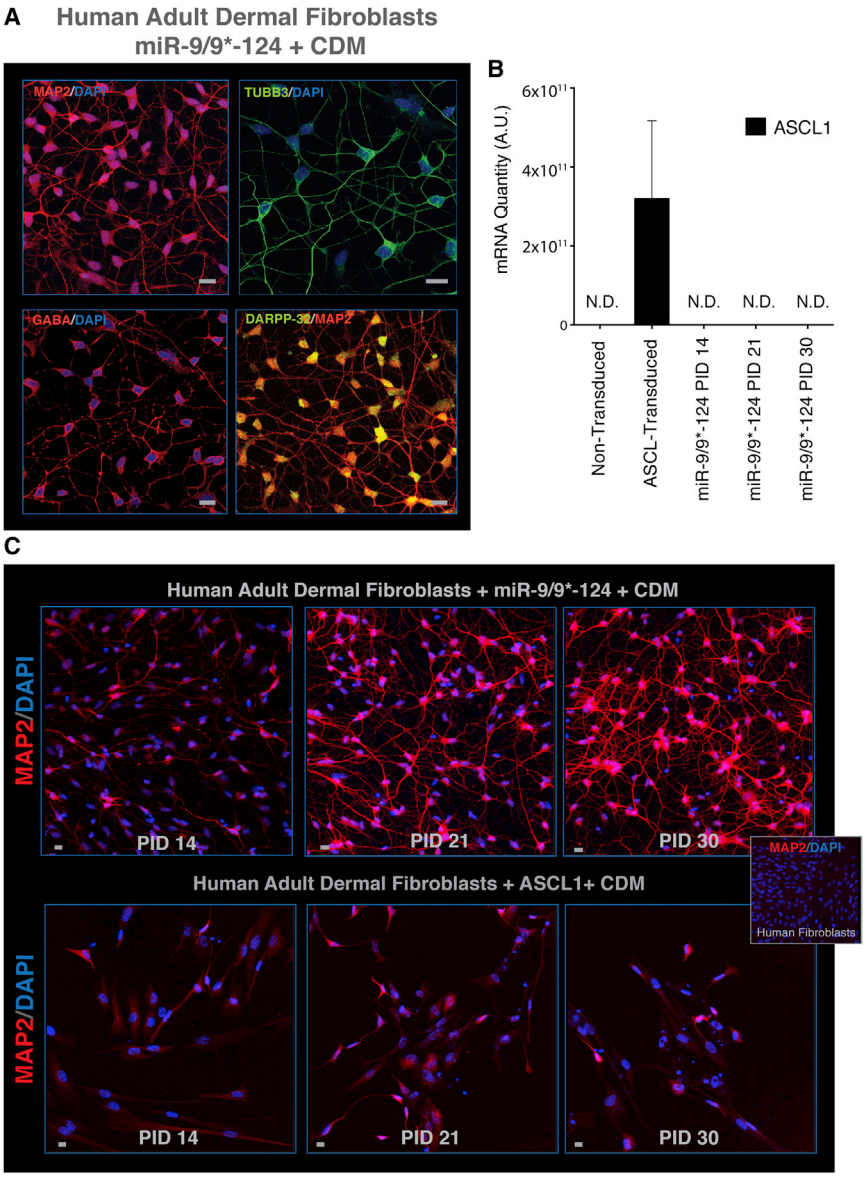

Figure 4. Conversion of Adult Human Fibroblasts Mediated by miR-9/9*-124 and Independent of ASCL1

(A) Expression of neuronal markers and markers of MSNs converted from adult human fibroblast (42 years old) transduced with miR-9/9*-124 + CDM. MAP2 (top left), TUBB3 (top right), GABA (bottom left), and DARPP-32 (bottom right).

(B) miR-9/9*-124-mediated neuronal reprogramming does not induce ASCL1 expression in human adult fibroblasts. miR-9/9*-124-expressing human adult fibroblasts were analyzed by qPCR at post-infection day (PID) 14, 21, and 30 for *ASCL1* expression. As a positive control, a separate preparation of human fibroblasts was transduced with ASCL1 cDNA, and RNA was collected after 48 hr. N.D., not detected. Error bars = SEM.

(C) Testing whether ASCL1 could substitute miR-9/9*-124 for neuronal reprogramming of human adult fibroblasts. Human adult fibroblasts were transduced with either miR-9/9*-124 + CDM (top pictures) or ASCL1 + CDM (bottom pictures) and immunostained for MAP2 at PID 14, 21, and 30. Based on the observation that MAP2-positive neuronal cells were largely absent in ASCL+CDM condition, miR-9/9*-124 is not interchangeable with ASCL1.

excitable, we also detected long delays to initial spike (Figure 3F) (6 out of 12 total cells recorded), a typical firing pattern of MSNs, whereas we only detected modest inward rectification (shown in Figure 3G and quantified in Figure 3H). We found that the degree of hyperpolarized resting membrane potential was minimal in tissue culture (−58.35 mV ± 3.08). The functional maturation of our cells from 6 to 12 weeks in monoculture (Figure S12) suggests that perhaps achieving a significantly hyperpolarized resting membrane potential requires longer culturing conditions. Consistently, MSNs from dissociated mouse striatal cultures have been shown to develop more negative membrane potentials with time in vitro (Lalchandani and Vicini, 2013).

Conversion of Adult Human Fibroblasts

Direct reprogramming of human postnatal and adult somatic cells into neurons has proved to be more challenging than reprogramming murine cells (Banito et al., 2009; Zhang et al., 2013). We asked whether the miR-9/9*-124-CDM-based approach could convert adult human fibroblasts into MSNs. We found that adult human dermal fibroblasts derived from a 42-year-old individual could be successfully converted into neurons with 82% of the cells being positive for MAP2 expression (n = 405 total cells) (representative image in Figure 4A). Consistent with the postnatal cells, the majority of adult cells were also GABAergic (86%, n = 147 total cells) and expressed DARPP-32 (77%, n = 333 total cells) (Figure 4A). In fact, we found that miR-9/9*-124 could reprogram human fibroblasts from multiple individuals independent of the donor's age with a similar efficiency (Figure S3).

The direct conversion of mouse fibroblasts into induced neurons has been reported with three transcription factors, BRN2, ASCL1, and MYT1L (Vierbuchen et al., 2010), while others have reprogrammed embryonic and fetal human fibroblasts with the same factors but supplemented with NeuroD1 (Pang et al., 2011; Son et al., 2011). Working solely with human postnatal fibroblasts, we showed that miR-9/9*-124 in combination with ASCL1, NEUROD2, and MYT1L successfully reprogramed fibroblasts into functional neurons (Yoo et al., 2011). The role for ASCL1 in direct neuronal reprogramming (Caiazzo et al., 2011; Pang et al., 2011; Yoo et al., 2011) has recently been reported to be due in part to its activity as a pioneer transcription factor (Wapinski et al., 2013), and we asked if

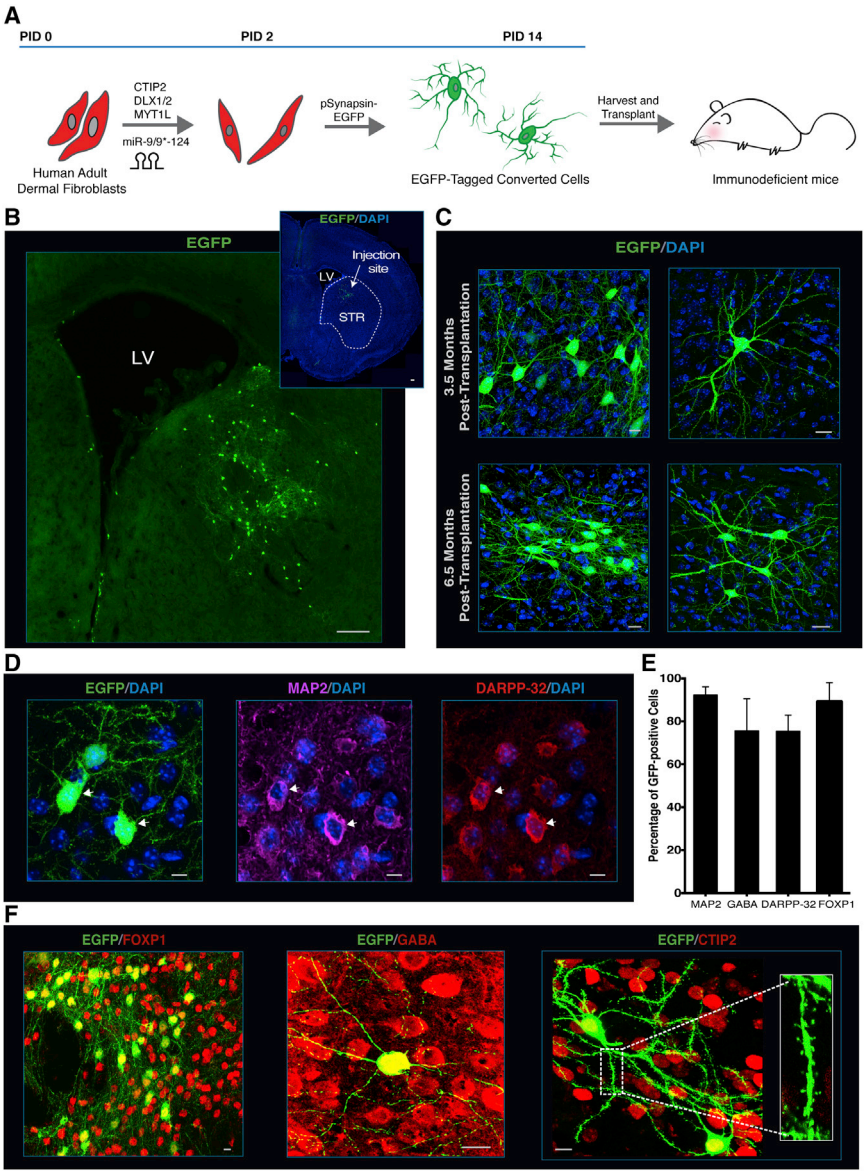

Figure 5. Engraftment and Long-Term Survival of Transplanted MSNs In Vivo

(A) A diagram illustrating our cell transplantation protocol. Human adult dermal fibroblasts were collected and cultured from a 22-year-old individual and transduced with lentivirus to express miR-9/9*-124 and CDM factors. At 2 days posttransduction, cells were transduced with additional lentivirus to label human cells with EGFP. At 2 weeks posttransduction, cells were harvested and transplanted into the striatum of NOD scid gamma immunodeficient mice.

(B) A low magnification of a coronal brain section showing transplanted human cells labeled with EGFP residing in the striatum. Scale bar, 80 μm. The inset displays a reconstruction of the coronal brain section with DAPI in blue.

LV, Lateral ventricle. STR, Striatum.

(C) Low- and high-magnification views of EGFP-positive cells in situ for 3.5 and 6.5 months posttransplantation. Scale bar, 10 μm.

(D) Expression of EGFP, MAP2, and DARPP-32. Arrows mark cells coexpressing all three markers. Scale bar, 10 μm.

(E) Quantification of MAP2, GABA and DARPP-32, and FOXP1-positive cells for EGFP-expressing cells. MAP2: n = 203 cells; GABA: n = 174 cells; DARPP-32: n = 173 cells; FOXP1: n = 173 cells. Error bars are in SD.

(F) Expression of FOXP1, GABA, and CTIP2 in miR-9/9*-124-CDM. Inset highlights dendritic spines. Scale bar, 10 μm.

miR-9/9*-124-mediated reprogramming involved the activity of ASCL1. We transduced human adult fibroblasts with miR-9/9*-124 to determine if *ASCL1* expression would be induced and found *ASCL1* expression to be undetectable upon the expression of miR-9/9*-124 at posttransduction days 14, 21, and 30 (Figure 4B). We also attempted to reprogram human adult fibroblasts into MSNs with CDM factors in conjunction with ASCL1. In comparison to miR-9/9*-124-CDM, ASCL1-CDM generated very few MAP2-positive cells that lacked neuronal morphologies (Figure 4C). Collectively, these findings indicate that miR-9/9*-124-mediated neuronal reprogramming is independent of the activity of ASCL1.

Functional Integration of Converted MSNs In Vivo

Next, we tested the ability of adult-derived cells to survive and differentiate in vivo by transplanting reprogrammed hMSNs into the mouse striatum. Adult fibroblasts were transduced with miR-9/9*-124-CDM and labeled with EGFP. Cells were harvested 2 weeks posttransduction, injected unilaterally into the striatum of immunodeficient mice and analyzed at day 50 after transplantation (DAT) (Figure 5A) (n = 14). EGFP-positive cells were detected in the dorsal striatum adjacent to the lateral ventricle (Figure 5B). Remarkably, we regularly detected EGFP cells in mice even after 3.5 and 6.5 months, demonstrating the stable conversion and long-term survival of the reprogrammed cells (Figure 5C). EGFP-marked cells were 93% MAP2 positive (n = 203), 76% GABAergic (n = 174), 91% DARPP-32 positive (n = 173), and 91% FOXP1 positive (n = 173) (Figures 5D, 5E, and 5F). Moreover, transplanted cells exhibited dense dendritic spines (Figure 5F, right).

Membrane Properties of Converted MSNs In Vivo

We assessed the functional properties of reprogrammed hMSNs in vivo in comparison to native mouse MSNs (mMSNs) using whole-cell recordings in acute striatal slices at 112 DAT (Figure 6A). A total of 18 cells were targeted for recordings, including 11 non-EGFP mMSNs and 7 EGFP-positive hMSNs. Native mMSNs were identified and distinguished from striatal interneurons based on their characteristic membrane properties and AP

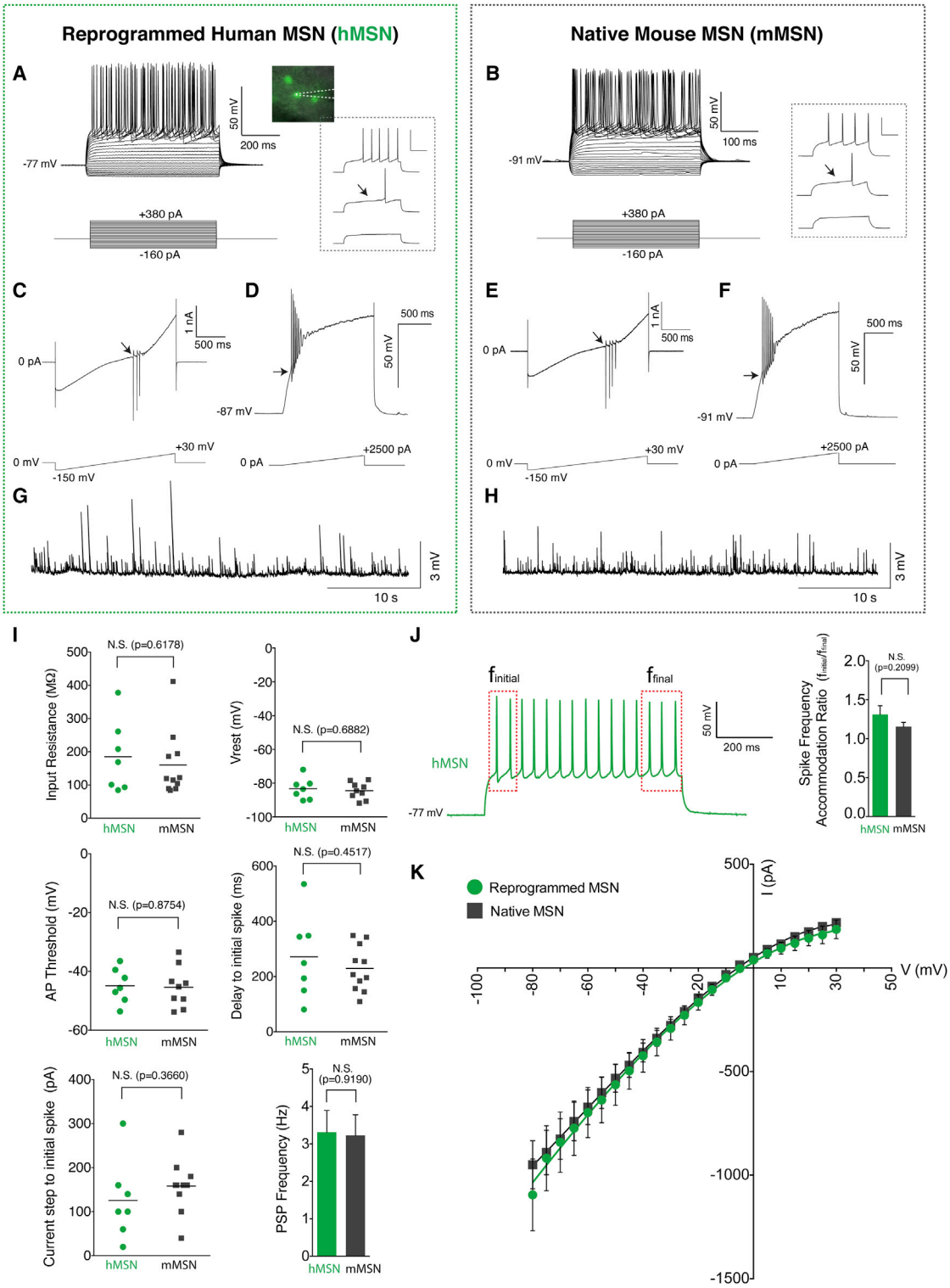

Figure 6. Functional Properties of Transplanted hMSNs in Comparison to mMSNs

(A and B) A total of 18 cells (7 EGFP-positive human cells and 11 non-EGFP mMSNs) were recorded from brains slices prepared at 16 weeks posttransplantation to compare membrane properties between reprogrammed human and mMSNs. AP trains were evoked by injecting current steps in EGFP-positive human cells (A) and mMSNs (B). The photograph depicts a representative image of whole-cell recording from an EGFP-positive cell in a striatal slice. Insets on the right show deconstructed traces of the first AP recorded, progressing from bottom to top. The arrows shown in the insets demonstrate delay to the initial spike, characteristic of MSNs. All 18 recorded cells were capable of generating repetitive APs.

(legend continued on next page)

firing patterns (Tepper et al., 2010). We found that all cells we examined (hMSNs and mMSNs) were able to fire AP trains when evoked by current steps and displayed long delays to initial AP spike (shown in the inset of Figures 6A and 6B and quantified in Figure 6I). Strong inward rectification, also characteristic of MSNs, was observed by an injection of voltage-ramp (Figure 6C for hMSNs and Figure 6E for mMSNs). The corresponding current-voltage relationship (I-V curve) was also identical between hMSNs and mMSNs (Figure 6K). Furthermore, we examined the AP threshold using a current-ramp protocol (Figure 6D for hMSNs and Figure 6F for mMSNs) and found no significant difference between the two cell types (Figure 6I). We then assessed whether transplanted cells were able to incorporate into local circuits by examining spontaneous postsynaptic potentials (sPSPs), which represent the network activity of surrounding neurons that form functional synapses onto hMSNs. As shown by the representative traces in Figures 6G and 6H, sPSPs were readily detected in all hMSNs (7 out of 7) and mMSNs (11 out of 11) with no significant difference in the sPSP frequency (Figure 6I), providing further evidence that transplanted cells could integrate into functional circuits in vivo. Additionally, we found that the resting membrane potentials of hMSNs were hyperpolarized (−83.29 mV ± 2.40) in hMSNs, similar to native mMSNs (−85.20 mV ± 1.67) (Figure 6I). We quantified the SFA ratio by calculating the frequency of the first spike ($F_{initial}$) in relation to the frequency of the average of the last two spike intervals (F_{final}), as previously reported (Venance and Glowinski, 2003). We found that both hMSNs and mMSNs displayed little to no spike accommodation with SFA values close to 1 (Figure 6J). Essentially, all membrane properties characteristic of MSNs that we analyzed were similar between transplanted and native MSNs during ex vivo recordings (Figure 6I).

Formation of Axonal Projections by Transplanted MSNs

Striatal MSNs give rise to projections terminating in two distinct nuclei within the basal ganglia, the globus pallidus and the substatia nigra, and these pair of nuclei in turn forms the two major striatal output systems (Gerfen, 1992). We therefore investigated whether transplanted hMSNs could extend projections into these distal targets of endogenous MSNs. Remarkably, we found EGFP-positive projections extending from the injection site in the dorsal striatum to the substantia nigra (six out of six brains analyzed at 56–64 DAT) with axon terminals also visible in the globus pallidus (Figure 7A). This finding signifies not only that reprogrammed hMSNs are capable of long distance axonal outgrowth but also that they recognize and follow axonal guidance cues intrinsic to striatal projection neurons. Interestingly, although transplanted hMSNs are mostly confined within 1 mm of the injection site (Figure 7B), we observed that a small number of cells (4.7%; n = 2,770 cells) could be found beyond the striatal boundary (Figure 7C). Due to the required transduction of multiple lentiviral vectors, we suspected that cells adopting positions outside the striatum lacked the expression of one or more factors. We found that while the vast majority of our EGFP-positive cells residing within the striatum expressed CTIP2, the occasional EGFP-positive cells found outside the striatum mostly lacked the expression of CTIP2 (92.3% n = 332) (Figure 7C). Since CTIP2 is highly expressed in the striatum as seen by immunostaining (Figure 7D), this finding may suggest that expression of CTIP2 may be important for determining migratory boundaries for cells destined to become MSNs within the developing striatum.

DISCUSSION

In this study, we describe a method to directly convert human postnatal and adult fibroblasts into a highly enriched population of striatal MSNs, the main cell type affected in Huntington's disease. We find that our direct reprogramming approach offers an unprecedented technological advance in time and homogeneity of generating DARPP-32-positive neurons in comparison to cells derived from iPSCs (HD iPSC Consortium, 2012; Zhang et al., 2010). In addition, we show that the reprogrammed cells have an analogous gene expression profile to primary hMSNs captured by laser microdissection and, when transplanted into the murine striatum, can functionally integrate into the local circuit, persist in situ for over 6 months, and send projections to correct anatomical targets. In previous studies, directly reprogrammed human neurons exhibited decreased competence for synapse formation, which hampered their use in disease modeling and made differentiating iPSCs or embryonic stem cells into neurons more appealing (Zhang et al., 2013). In our current study, we present evidence that miRNA-dependent direct reprogramming generates functional neurons readily capable to form synapses in vivo. Lastly, our results demonstrate that miR-9/9*-124-CDM-mediated derivation of MSNs from human skin fibroblasts is efficient and consistent in multiple samples from postnatal to adult individuals.

The authenticity of our converted MSNs is likely due to the combinatorial code for gene expression generated by miR-9/9*-124-CDM, which resembles the endogenous cell differentiation program of MSNs. We paid particular attention to factors that could be instructive in defining different stages of the striatal

(C–F) Voltage ramp protocol from −150 mV to +30 mV shows inward rectification at hyperpolarized membrane potentials and outward currents as cells become depolarized in reprogrammed human cells (C) and mMSNs (E). Large inward currents can be seen as the cell reaches AP threshold (arrows). AP threshold was measured by assessing APs occurring with steady-state current injections in reprogrammed hMSNs (D) and mMSNs (F). Arrows demonstrate the onset of APs. (G and H) Representative traces of sPSPs recorded from transplanted human cells (G) and mMSNs (H). Seven out of seven EGFP-positive cells, and all mMSNs, displayed spontaneous PSPs. sPSP frequencies are quantified in the last graph of (I).

(I) Comparative analyses of active and passive membrane properties between hMSNs and mMSNs. Similar membrane properties were observed in all quantified properties, including input resistance, resting membrane potential (Vrest), AP threshold, delay time to initial spikes, current steps to initial spike, and PSP frequencies shown in (G) and (H). Individual data points are presented to show the degree of deviation from the mean. Histogram shown as mean ± SEM. N.S., not significant by student t test.

(J) A representative AP trace from a hMSN illustrating the frequency ratio ($f_{initial}/f_{final}$) to determine SFAs, quantified at 40 pA above AP threshold. Histogram on the right shows no significant difference between hMSNs and mMSNs. Data presented as mean ± SEM.

(K) I-V curves for hMSNs in green and mMSNs in gray, demonstrating large inward rectifications at hyperpolarized membrane potentials for both cases.

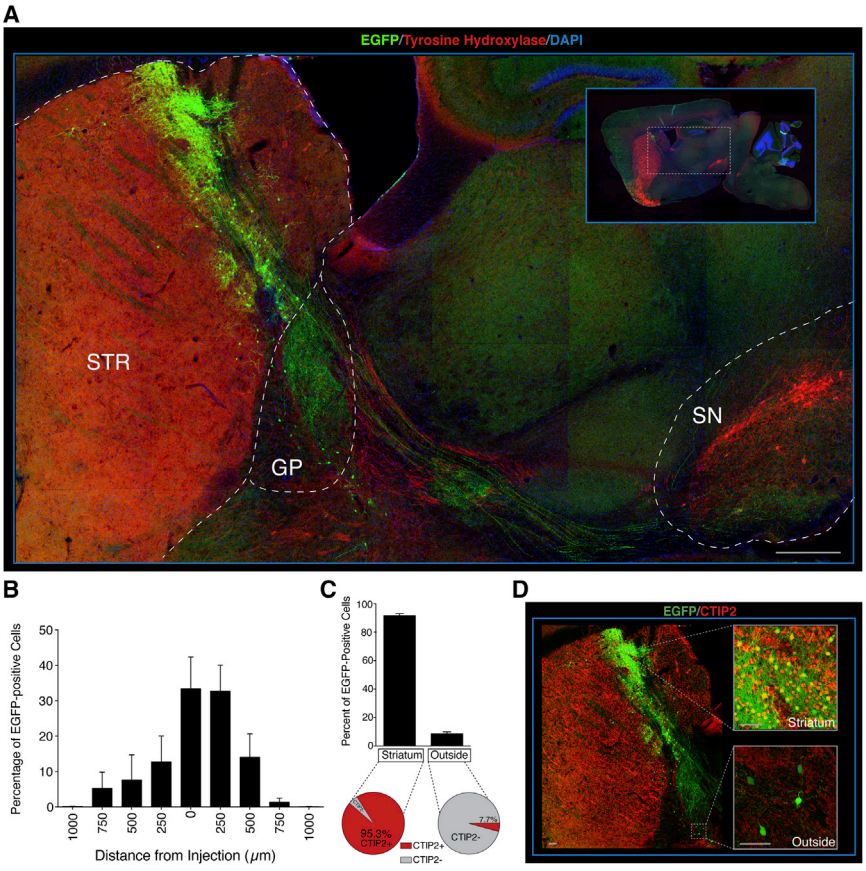

Figure 7. Establishment and Targeting of Axonal Projections by Transplanted HMSNs

(A) Midsagittal brain section immunostained with tyrosine hydroxylase in red labeling cell bodies in the substatia nigra (SN) and its dense innervation of the striatum (STR). EGFP-positive cells and dendrites can be seen dispersed throughout the dorsal striatum with projections extending to globus pallidus (GP) and substantia nigra (SN) in green. Scale bar, 300 μm.

(B) Quantification of cell migration in the medial-lateral axis from the injection site represented in the histogram as 0 μm. n = 3 animals with a total of 2,770 cells counted.

(C and D) The vast majority of EGFP-positive cells were confined within the striatum (95.3%), while a small population of cells was found beyond the striatal boundary (n = 2,770 cells counted for striatum versus outside) (C). While the vast majority of the EGFP-positive cells within the striatum were CTIP2 positive, nearly all the EGFP-positive cells found outside of the striatum lacked the expression of CTIP2 (quantified in the gray are of the pie chart in [C] and pictured in [D]). n = 332 cells. Scale bar, 30 μm. Error bars = SEM.

cell lineage. For example, the expression of DLX1/2 in the absence of ASCL1 is known to form GABAergic neurons that originate from the same birthplace as MSNs, the ganglionic eminence of the ventral forebrain (Letinic et al., 2002). Later, as MSNs migrate away from the ganglionic eminence into the striatum, CTIP2 begins to be expressed and is maintained at high levels throughout adulthood (Arlotta et al., 2008). Similarly, the cells undergoing neuronal reprogramming were likely poised to a neuronal state by miR-9/9*-124 and MYT1L and refined to adopt a fate analogous to MSNs by the instruction of DLX1/2 and CTIP2. This process can be compared to a recent proposal that the attainment of a stable neuronal cell identity occurs in progressive steps in which a common neuronal identity is established first, and only after the initiation of refinement programs, a neuron becomes terminally differentiated (Fishell and Heintz, 2013). Similarly, we postulate that miR-9/9*-124 drives human fibroblasts into a neuronal state that can be further modulated by the instruction of lineage-specific fate determinants. This miR-9/9*-124-induced neuronal state can be characterized by (I) induction of proliferative cells to become post-mitotic, (II) acquisition of neuronal morphology, (III) induction of broadly expressed neuronal markers (MAP2, TUBB3, and NeuN) lacking markers of neuronal subtypes, (IV) induction of compositional changes in the neuron-specific BAF (nBAF) chromatin remodeling complexes (Staahl et al., 2013; Yoo et al., 2009), and lastly, (V) suppression of factors that antagonize the expression of neuron-specific genes, such as the RE1-silencing transcription factor (REST/NRSF) and PTBP1 (Boutz et al., 2007; Conaco et al., 2006; Makeyev et al., 2007; Packer et al., 2008; Xue et al., 2013). In our current study, the overexpression of CDM was only capable of generating neurons when coexpressed with miR-9/9*-124, suggesting that these miRNAs promote a neuronal state permissive for the activity of terminal fate determinants. We postulate that this neuronal state may be, at least partially, due to the ability of miR-9/9*-124 to alter the chromatin landscape of non-neuronal cells during neural induction. Namely, miR-9/9* and miR-124 have been shown to regulate the activity of REST/NRSF complex (Packer et al., 2008; Visvanathan et al., 2007), which blocks the expression of neuronal genes in non-neuronal cells by recruiting and assembling a multimeric repressor complex composed of epigenetic regulatory factors (Ballas and Mandel, 2005). Therefore, the ectopic expression of miR-9/9*, which directly suppresses REST/NRSF, and miR-124, which targets the antineural factors PTPB1 and SCP1, results in activation of neuronal genes (Makeyev et al., 2007; Packer et al., 2008; Visvanathan et al., 2007). Importantly, miR-9/9*-124 orchestrate the switch of subunits of BAF chromatin remodeling complexes to promote a nBAF complex, an evolutionarily conserved process crucial for postmitotic neural development and dendritic morphogenesis (Yoo et al., 2009). It is interesting to note that REST-mediated neuronal gene repression has been demonstrated to be dependent on the activity of the BAF chromatin-remodeling complexes (Battaglioli et al., 2002). Even more intriguingly, CTIP2 (BCL11B) has recently been found to be a dedicated and stable subunit of the BAF complex (Kadoch et al., 2013). The ectopic expression of miR-9/9*-124 in conjunction with CTIP2 therefore is likely to shape the activity of the BAF complex and could potentially

explain our robust reprogramming toward a DARPP-32-positive cell fate, although this remains speculative. Collectively, the changes mediated by miR-9/9*-124 poise the cell to adopt a neurogenic state that can be influenced by lineage-specific transcription factors to guide neuronal conversion toward specific subtypes, as demonstrated in our study.

Moreover, we observed that several individual transcription factors besides CDM factors could robustly generate MAP2-positive human cells with miR-9/9*-124, although the subtype identify of these neurons are yet to be determined (Figure S3). This finding raises the possibility of simply fine-tuning the composition of additional transcription factors to generate various neuronal subtypes. Since our current study suggests that miR-9/9*-124-mediated reprogramming is independent of ASCL1, miR-9/9*-124-based reprogramming may be beneficial for inducing neuronal subtypes that do not contain ASCL1 in their endogenous differentiation program. Alternatively, ASCL1 may be combined with miR-9/9*-124 to derive neuronal subtypes where ASCL1 is involved in terminal differentiation. In summary, our study utilizing the neurogenic activities of microRNAs and transcription factors demonstrates an important step toward generating human neurons of a specific neuronal subtype, an experimental approach of extreme importance when studying neurological diseases affecting specific neuronal subtypes and brain regions.

EXPERIMENTAL PROCEDURES

Cell Culture

Lentiviral preparation of a Dox-responsive synthetic cluster of miR-9/9* and miR-124 (Yoo et al., 2011), as well as transcription factors cloned downstream of the EF1α promoter, was used to transduce human postnatal or adult fibroblasts (ATCC and ScienCell). The following cell line was obtained from the NIGMS Human Genetic Cell Repository at the Coriell Institute for Medical Research: GM02171 and used for data shown in Figures 5 and S3 (C). Typically, infected human fibroblasts were maintained in fibroblast media for 2 days with Dox before replating onto coated coverslips. Cells were then selected with appropriate antibiotics in neuronal media (ScienCell) supplemented with valproic acid (1 mM), dibutyryl cAMP (200 μM), BDNF (10 ng/ml), NT-3 (10 ng/ml), and RA (1 μM). Dox was replenished every 2 days and media were changed every 4 days. A detailed reprogramming protocol is available in Supplemental Experimental Procedures.

Immunofluorescence

Cells were fixed using 4% paraformaldehyde or combined with 0.2% glutaraldehyde (both from Electron Microscopy Sciences) for 20 min at room temperature (RT) followed by permeabilization with 0.2% Triton X-100 for 10 min. One percent goat or donkey serum was used for blocking followed by incubation of primary antibodies overnight at 4°C. Secondary antibodies conjugated to Alexa-488, -594, or -647 were applied for 1 hr at RT. Detailed list of antibodies used and the procedure for immunohistochemistry analysis can be found in the Supplemental Experimental Procedures.

Single-Cell Quantitative PCR

Reprogrammed postnatal cells were harvested and single cells were collected by FACS sorting 5 weeks posttransduction. Deidentified human striatal sections from postmortem autopsy samples were obtained in accordance with the guideline of HRPO of Washington University School of Medicine. Postmortem single cells stained with cresyl violet were laser dissected from striatal putamen tissue sections of an 89-year-old individual. Samples were used for reverse-transcription and gene expression analysis using Fluidigm Dynamic arrays (see Supplemental Experimental Procedures).

Cell Harvesting and Transplantation

Reprogrammed cells were typically transduced with a Synapsin promoter-EGFP lentivirus at reprogramming day 2 and harvested for transplantation studies at reprogramming day 14. Adherent cell cultures were mechanically dissociated and concentrated by centrifugation (4 min at 1,000 RPM). Concentrated cell suspensions ($\sim 10^4$ cells/μl) were loaded into a 5 μl Hamilton syringe (26 s/2/2 Gauge/Length/Point) and 2 μl injected into the right striatum of NSG mice (P0 to P1).

Animals

Mice were maintained in standard housing conditions with food and water provided ad libitum. All procedures followed the guidelines of the Washington University's Institutional Animal Care and Use Committee (IACUC) and the Animal Studies Committee (ASC).

Electrophysiology, Slice Preparation, and Recordings

Detailed methods and description of the composition of internal and external solutions used for ex vivo recording can be found in the Supplemental Experimental Procedures.

SUPPLEMENTAL INFORMATION

Supplemental Information includes twelve figures, two tables, and Supplemental Experimental Procedures and can be found with this article online at http://dx.doi.org/10.1016/j.neuron.2014.10.016.

AUTHOR CONTRIBUTIONS

M.B.V., M.R., and A.S.Y. generated the hypotheses, designed experiments and wrote the manuscript. M.R. performed reprogramming experiments. M.B.V. generated data in Figures 3–7 and supplemental figures. C.S. generated data shown in Figure 3. A.S.Y. and M.R. generated data shown in Figure 2. J.M.N., T.O.H., and J.L.R. generated data in Figure 6. P.Y.D. and V.A.K piloted in vivo electrophysiology experiments.

ACKNOWLEDGMENTS

We thank S. Dahiya and C. Huh for providing human striatum sections and performing laser microdissections and A. Soleiman for technical assistance. We thank J.D. Surmeier, S. Zakharenko, S. Mennerick, L. Solica-Krezel, and D. Abernathy for helpful suggestions with the manuscript; the Genome Technology Access Center in the Department of Genetics at Washington University School of Medicine for help with single-cell analysis; J. Ho and J. Richner for help with FACS sorting; and J. Dougherty for TRAP data analysis. M.B.V. is supported by the National Science Foundation Graduate Research Fellowship (DGE-1143954). C.S. is supported by the fellowship from Cognitive, Computational and Systems Neuroscience Pathway (T32N5023547) and a grant from NIH, MH078823. J.M.N. is supported by the National Institute of General Medical Sciences (R01 GM104991) and the National Heart Lung and Blood Institute (T.O.H. is supported by T32 HL007275). A.S.Y. is supported by NIH Director's Innovator Award (DP2) and awards from the Mallinckrodt Jr. Foundation, Ellison Medical Foundation, and Presidential Early Career Award for Scientists and Engineers.

Accepted: October 6, 2014
Published: October 22, 2014

REFERENCES

Alavian, K.N., Li, H., Collis, L., Bonanni, L., Zeng, L., Sacchetti, S., Lazrove, E., Nabili, P., Flaherty, B., Graham, M., et al. (2011). Bcl-xL regulates metabolic efficiency of neurons through interaction with the mitochondrial F1FO ATP synthase. Nat. Cell Biol. *13*, 1224–1233.

Albin, R.L., Young, A.B., and Penney, J.B. (1989). The functional anatomy of basal ganglia disorders. Trends Neurosci. *12*, 366–375.

Albu, D.I., Feng, D., Bhattacharya, D., Jenkins, N.A., Copeland, N.G., Liu, P., and Avram, D. (2007). BCL11B is required for positive selection and survival of double-positive thymocytes. J. Exp. Med. *204*, 3003–3015.

Anderson, S.A., Qiu, M., Bulfone, A., Eisenstat, D.D., Meneses, J., Pedersen, R., and Rubenstein, J.L. (1997). Mutations of the homeobox genes Dlx-1 and Dlx-2 disrupt the striatal subventricular zone and differentiation of late born striatal neurons. Neuron *19*, 27–37.

Arlotta, P., Molyneaux, B.J., Jabaudon, D., Yoshida, Y., and Macklis, J.D. (2008). Ctip2 controls the differentiation of medium spiny neurons and the establishment of the cellular architecture of the striatum. J. Neurosci. *28*, 622–632.

Ballas, N., and Mandel, G. (2005). The many faces of REST oversee epigenetic programming of neuronal genes. Curr. Opin. Neurobiol. *15*, 500–506.

Banito, A., Rashid, S.T., Acosta, J.C., Li, S., Pereira, C.F., Geti, I., Pinho, S., Silva, J.C., Azuara, V., Walsh, M., et al. (2009). Senescence impairs successful reprogramming to pluripotent stem cells. Genes Dev. *23*, 2134–2139.

Battaglioli, E., Andrés, M.E., Rose, D.W., Chenoweth, J.G., Rosenfeld, M.G., Anderson, M.E., and Mandel, G. (2002). REST repression of neuronal genes requires components of the hSWI.SNF complex. J. Biol. Chem. *277*, 41038–41045.

Blömer, U., Kafri, T., Randolph-Moore, L., Verma, I.M., and Gage, F.H. (1998). Bcl-xL protects adult septal cholinergic neurons from axotomized cell death. Proc. Natl. Acad. Sci. USA *95*, 2603–2608.

Boutz, P.L., Stoilov, P., Li, Q., Lin, C.H., Chawla, G., Ostrow, K., Shiue, L., Ares, M., Jr., and Black, D.L. (2007). A post-transcriptional regulatory switch in polypyrimidine tract-binding proteins reprograms alternative splicing in developing neurons. Genes Dev. *21*, 1636–1652.

Caiazzo, M., Dell'Anno, M.T., Dvoretskova, E., Lazarevic, D., Taverna, S., Leo, D., Sotnikova, T.D., Menegon, A., Roncaglia, P., Colciago, G., et al. (2011). Direct generation of functional dopaminergic neurons from mouse and human fibroblasts. Nature *476*, 224–227.

Conaco, C., Otto, S., Han, J.J., and Mandel, G. (2006). Reciprocal actions of REST and a microRNA promote neuronal identity. Proc. Natl. Acad. Sci. USA *103*, 2422–2427.

HD iPSC Consortium (2012). Induced pluripotent stem cells from patients with Huntington's disease show CAG-repeat-expansion-associated phenotypes. Cell Stem Cell *11*, 264–278.

Desplats, P.A., Kass, K.E., Gilmartin, T., Stanwood, G.D., Woodward, E.L., Head, S.R., Sutcliffe, J.G., and Thomas, E.A. (2006). Selective deficits in the expression of striatal-enriched mRNAs in Huntington's disease. J. Neurochem. *96*, 743–757.

Do, J., Kim, J.I., Bakes, J., Lee, K., and Kaang, B.K. (2012). Functional roles of neurotransmitters and neuromodulators in the dorsal striatum. Learn. Mem. *20*, 21–28.

Dougherty, J.D., Schmidt, E.F., Nakajima, M., and Heintz, N. (2010). Analytical approaches to RNA profiling data for the identification of genes enriched in specific cells. Nucleic Acids Res. *38*, 4218–4230.

Ferland, R.J., Cherry, T.J., Preware, P.O., Morrisey, E.E., and Walsh, C.A. (2003). Characterization of Foxp2 and Foxp1 mRNA and protein in the developing and mature brain. J. Comp. Neurol. *460*, 266–279.

Fishell, G., and Heintz, N. (2013). The neuron identity problem: form meets function. Neuron *80*, 602–612.

Gerfen, C.R. (1992). The neostriatal mosaic: multiple levels of compartmental organization in the basal ganglia. Annu. Rev. Neurosci. *15*, 285–320.

Gertler, T.S., Chan, C.S., and Surmeier, D.J. (2008). Dichotomous anatomical properties of adult striatal medium spiny neurons. J. Neurosci. *28*, 10814–10824.

Gong, S., Zheng, C., Doughty, M.L., Losos, K., Didkovsky, N., Schambra, U.B., Nowak, N.J., Joyner, A., Leblanc, G., Hatten, M.E., and Heintz, N. (2003). A gene expression atlas of the central nervous system based on bacterial artificial chromosomes. Nature *425*, 917–925.

Graybiel, A.M., Aosaki, T., Flaherty, A.W., and Kimura, M. (1994). The basal ganglia and adaptive motor control. Science *265*, 1826–1831.

Hobert, O. (2011). Regulation of terminal differentiation programs in the nervous system. Annu. Rev. Cell Dev. Biol. *27*, 681–696.

Hu, B.Y., Weick, J.P., Yu, J., Ma, L.X., Zhang, X.Q., Thomson, J.A., and Zhang, S.C. (2010). Neural differentiation of human induced pluripotent stem cells follows developmental principles but with variable potency. Proc. Natl. Acad. Sci. USA *107*, 4335–4340.

Johnston, J.G., Gerfen, C.R., Haber, S.N., and van der Kooy, D. (1990). Mechanisms of striatal pattern formation: conservation of mammalian compartmentalization. Brain Res. Dev. Brain Res. *57*, 93–102.

Kadoch, C., Hargreaves, D.C., Hodges, C., Elias, L., Ho, L., Ranish, J., and Crabtree, G.R. (2013). Proteomic and bioinformatic analysis of mammalian SWI/SNF complexes identifies extensive roles in human malignancy. Nat. Genet. *45*, 592–601.

Karl, C., Couillard-Despres, S., Prang, P., Munding, M., Kilb, W., Brigadski, T., Plötz, S., Mages, W., Luhmann, H., Winkler, J., et al. (2005). Neuronal precursor-specific activity of a human doublecortin regulatory sequence. J. Neurochem. *92*, 264–282.

Koós, T., and Tepper, J.M. (1999). Inhibitory control of neostriatal projection neurons by GABAergic interneurons. Nat. Neurosci. *2*, 467–472.

Kreitzer, A.C. (2009). Physiology and pharmacology of striatal neurons. Annu. Rev. Neurosci. *32*, 127–147.

Lalchandani, R.R., and Vicini, S. (2013). Inhibitory collaterals in genetically identified medium spiny neurons in mouse primary corticostriatal cultures. Physiol. Rep. Published online November 24, 2013. http://dx.doi.org/10.1002/phy2.164.

Lapasset, L., Milhavet, O., Prieur, A., Besnard, E., Babled, A., Aït-Hamou, N., Leschik, J., Pellestor, F., Ramirez, J.M., De Vos, J., et al. (2011). Rejuvenating senescent and centenarian human cells by reprogramming through the pluripotent state. Genes Dev. *25*, 2248–2253.

Letinic, K., Zoncu, R., and Rakic, P. (2002). Origin of GABAergic neurons in the human neocortex. Nature *417*, 645–649.

Liu, M.L., Zang, T., Zou, Y., Chang, J.C., Gibson, J.R., Huber, K.M., and Zhang, C.L. (2013). Small molecules enable neurogenin 2 to efficiently convert human fibroblasts into cholinergic neurons. Nat. Commun. *4*, http://dx.doi.org/10.1038/ncomms3183.

Lobo, M.K., Karsten, S.L., Gray, M., Geschwind, D.H., and Yang, X.W. (2006). FACS-array profiling of striatal projection neuron subtypes in juvenile and adult mouse brains. Nat. Neurosci. *9*, 443–452.

Makeyev, E.V., Zhang, J., Carrasco, M.A., and Maniatis, T. (2007). The MicroRNA miR-124 promotes neuronal differentiation by triggering brain-specific alternative pre-mRNA splicing. Mol. Cell *27*, 435–448.

Marin, O., Anderson, S.A., and Rubenstein, J.L. (2000). Origin and molecular specification of striatal interneurons. J. Neurosci. *20*, 6063–6076.

Miller, J.D., Ganat, Y.M., Kishinevsky, S., Bowman, R.L., Liu, B., Tu, E.Y., Mandal, P.K., Vera, E., Shim, J.W., Kriks, S., et al. (2013). Human iPSC-based modeling of late-onset disease via progerin-induced aging. Cell Stem Cell *13*, 691–705.

Ouimet, C.C., and Greengard, P. (1990). Distribution of DARPP-32 in the basal ganglia: an electron microscopic study. J. Neurocytol. *19*, 39–52.

Packer, A.N., Xing, Y., Harper, S.Q., Jones, L., and Davidson, B.L. (2008). The bifunctional microRNA miR-9/miR-9* regulates REST and CoREST and is downregulated in Huntington's disease. J. Neurosci. *28*, 14341–14346.

Pang, Z.P., Yang, N., Vierbuchen, T., Ostermeier, A., Fuentes, D.R., Yang, T.Q., Citri, A., Sebastiano, V., Marro, S., Südhof, T.C., and Wernig, M. (2011). Induction of human neuronal cells by defined transcription factors. Nature *476*, 220–223.

Peça, J., Feliciano, C., Ting, J.T., Wang, W., Wells, M.F., Venkatraman, T.N., Lascola, C.D., Fu, Z., and Feng, G. (2011). Shank3 mutant mice display autistic-like behaviours and striatal dysfunction. Nature *472*, 437–442.

Pert, C.B., Kuhar, M.J., and Snyder, S.H. (1976). Opiate receptor: autoradiographic localization in rat brain. Proc. Natl. Acad. Sci. USA *73*, 3729–3733.

Ring, K.L., Tong, L.M., Balestra, M.E., Javier, R., Andrews-Zwilling, Y., Li, G., Walker, D., Zhang, W.R., Kreitzer, A.C., and Huang, Y. (2012). Direct reprogramming of mouse and human fibroblasts into multipotent neural stem cells with a single factor. Cell Stem Cell *11*, 100–109.

Sahay, A., Scobie, K.N., Hill, A.S., O'Carroll, C.M., Kheirbek, M.A., Burghardt, N.S., Fenton, A.A., Dranovsky, A., and Hen, R. (2011). Increasing adult hippocampal neurogenesis is sufficient to improve pattern separation. Nature *472*, 466–470.

Soldner, F., and Jaenisch, R. (2012). Medicine. iPSC disease modeling. Science *338*, 1155–1156.

Son, E.Y., Ichida, J.K., Wainger, B.J., Toma, J.S., Rafuse, V.F., Woolf, C.J., and Eggan, K. (2011). Conversion of mouse and human fibroblasts into functional spinal motor neurons. Cell Stem Cell *9*, 205–218.

Staahl, B.T., Tang, J., Wu, W., Sun, A., Gitler, A.D., Yoo, A.S., and Crabtree, G.R. (2013). Kinetic analysis of npBAF to nBAF switching reveals exchange of SS18 with CREST and integration with neural developmental pathways. J. Neurosci. *33*, 10348–10361.

Stenman, J., Toresson, H., and Campbell, K. (2003). Identification of two distinct progenitor populations in the lateral ganglionic eminence: implications for striatal and olfactory bulb neurogenesis. J. Neurosci. *23*, 167–174.

Takahashi, K., and Yamanaka, S. (2006). Induction of pluripotent stem cells from mouse embryonic and adult fibroblast cultures by defined factors. Cell *126*, 663–676.

Tamura, S., Morikawa, Y., Iwanishi, H., Hisaoka, T., and Senba, E. (2004). Foxp1 gene expression in projection neurons of the mouse striatum. Neuroscience *124*, 261–267.

Tepper, J.M., Tecuapetla, F., Koos, T., and Ibanez-Sandoval, O. (2010). Heterogeneity and diversity of striatal GABAergic interneurons. Front. Neuroanat. *4*, http://dx.doi.org/10.3389/fnana.2010.00150.

Venance, L., and Glowinski, J. (2003). Heterogeneity of spike frequency adaptation among medium spiny neurones from the rat striatum. Neuroscience *122*, 77–92.

Vierbuchen, T., Ostermeier, A., Pang, Z.P., Kokubu, Y., Südhof, T.C., and Wernig, M. (2010). Direct conversion of fibroblasts to functional neurons by defined factors. Nature *463*, 1035–1041.

Visvanathan, J., Lee, S., Lee, B., Lee, J.W., and Lee, S.K. (2007). The microRNA miR-124 antagonizes the anti-neural REST/SCP1 pathway during embryonic CNS development. Genes Dev. *21*, 744–749.

Wapinski, O.L., Vierbuchen, T., Qu, K., Lee, Q.Y., Chanda, S., Fuentes, D.R., Giresi, P.G., Ng, Y.H., Marro, S., Neff, N.F., et al. (2013). Hierarchical mechanisms for direct reprogramming of fibroblasts to neurons. Cell *155*, 621–635.

Xue, Y., Ouyang, K., Huang, J., Zhou, Y., Ouyang, H., Li, H., Wang, G., Wu, Q., Wei, C., Bi, Y., et al. (2013). Direct conversion of fibroblasts to neurons by reprogramming PTB-regulated microRNA circuits. Cell *152*, 82–96.

Yoo, A.S., Staahl, B.T., Chen, L., and Crabtree, G.R. (2009). MicroRNA-mediated switching of chromatin-remodelling complexes in neural development. Nature *460*, 642–646.

Yoo, A.S., Sun, A.X., Li, L., Shcheglovitov, A., Portmann, T., Li, Y., Lee-Messer, C., Dolmetsch, R.E., Tsien, R.W., and Crabtree, G.R. (2011). MicroRNA-mediated conversion of human fibroblasts to neurons. Nature *476*, 228–231.

Yu, J., Vodyanik, M.A., Smuga-Otto, K., Antosiewicz-Bourget, J., Frane, J.L., Tian, S., Nie, J., Jonsdottir, G.A., Ruotti, V., Stewart, R., et al. (2007). Induced pluripotent stem cell lines derived from human somatic cells. Science *318*, 1917–1920.

Zhang, R., Xue, Y.Y., Lu, S.D., Wang, Y., Zhang, L.M., Huang, Y.L., Signore, A.P., Chen, J., and Sun, F.Y. (2006). Bcl-2 enhances neurogenesis and inhibits apoptosis of newborn neurons in adult rat brain following a transient middle cerebral artery occlusion. Neurobiol. Dis. *24*, 345–356.

Zhang, N., An, M.C., Montoro, D., and Ellerby, L.M. (2010). Characterization of Human Huntington's Disease Cell Model from Induced Pluripotent Stem Cells. PLoS Curr. *2*, RRN1193.

Zhang, Y., Pak, C., Han, Y., Ahlenius, H., Zhang, Z., Chanda, S., Marro, S., Patzke, C., Acuna, C., Covy, J., et al. (2013). Rapid single-step induction of functional neurons from human pluripotent stem cells. Neuron *78*, 785–798.